RESEARCH ARTICLE

Rising Stars

ADVANCED OPTICAL MATERIALS
www.advopticalmat.de

Near-Infrared Metalens Empowered Dual-Mode High Resolution and Large FOV Microscope

Chuang Sun, Hailong Pi, Kian Shen Kiang, Jize Yan, and Jun-Yu Ou**

The spiral phase contrast microscope can clearly distinguish the morphological information of the low contrast objects (i.e., biological samples) owing to the isotropic edge-enhancement effect, while the bright field microscope can image the overall morphology of amplitude objects. However, the imaging resolution, magnification, and field of view of conventional spiral phase contrast microscopes based on 4f filtering configuration are limited by the system's complexity. Here, compact dual-mode microscopes working at near-infrared using the engineered metalens are reported, which can be tuned between the spiral phase contrast imaging and bright field imaging by polarization control. The metalens combine the high-resolution objective lens and polarization-controlled phase filter into a single-layer nanofins array. Two infinity-corrected microscope systems are demonstrated to achieve subwavelength resolution (0.7λ), large magnification (58X), and large field of view (600 × 800 µm). Unstained onion epidermal is imaged by the microscope to show the dual-mode imaging ability for the biological sample. Finally, a singlet dual-mode microscope system is demonstrated to show the edge-detection application for industrial standards. These results can open new opportunities in applications of biological imaging, industrial machine vision, and semiconductor inspection.

1. Introduction

Bright-field microscope is widely used for imaging the overall morphologies of amplitude objects. However, the bright field microscope cannot provide clearly distinguished morphological information of the transparent objects (i.e., low index contrast objects).[1] To realize high-contrast and edge-enhanced imaging of phase objects, a phase contrast microscope was introduced by the Dutch physicist Frits Zernike in the 1930s.[2,3] Compared with algorithm-based edge enhancement image processing, a phase contrast microscope is an all-optical processing and could provide direct edge detection functionality.[4] This technique is used for high-contrast imaging of transparent specimens, including living cells (typically in culture), unstained biological samples, and microorganisms and for low optical-contrast specimens.[5]

Essentially, a phase contrast microscope is based on filtering image information in its Fourier plane (i.e., frequency domain).[3] As the spiral phase filtering function can lead to a 2D isotropic edge-enhancement effect in amplitude and phase objects, the spiral phase contrast microscope has been implemented in many ways. Conventionally, the spiral phase contrast microscope is implemented by generating a spiral phase profile at the Fourier plane of a 4f filtering system via a spatial light modulate, which makes the microscope system too bulky and limits the resolution and field of view (FOV).[6,7]

In recent years, metasurfaces made from arrays of subwavelength nanofins have attracted a lot of attention in the imaging community because of their powerful ability to manipulate amplitude, phase, and polarization of incident light on demand.[8–11] A transmissive dielectric metasurface working as a polarization-controlled phase filter is placed in the Fourier plane of a 4f system for realizing switchable spiral phase contrast imaging.[12] Additionally, reflection configurations based on reflective metasurfaces are proposed as well.[13–14] However, the multiple lenses used in both 4f filtering system or reflection configuration result in a complex and bulky optical system, which fails to exploit the multi-functional merit of a metasurface and hinders the miniaturization of the spiral phase contrast imaging system. Based on the second-order derivative theory, an optical differentiator is obtained via a metasurface for realizing the 2D edge detection.[15] However, an additional microscope system is needed to achieve the edge-enhanced image because the optical differentiator cannot serve as an imaging lens. Inspired by the differential interference contrast microscope, a quantitative

C. Sun, H. Pi, K. S. Kiang, J. Yan
School of Electronics and Computer Science
University of Southampton
Southampton SO17 1BJ, UK
E-mail: J.Yan@soton.ac.uk

J.-Y. Ou
Department of Physics and Astronomy
University of Southampton
Southampton SO17 1BJ, UK
E-mail: bruce.ou@soton.ac.uk

The ORCID identification number(s) for the author(s) of this article can be found under https://doi.org/10.1002/adom.202400512

DOI: 10.1002/adom.202400512

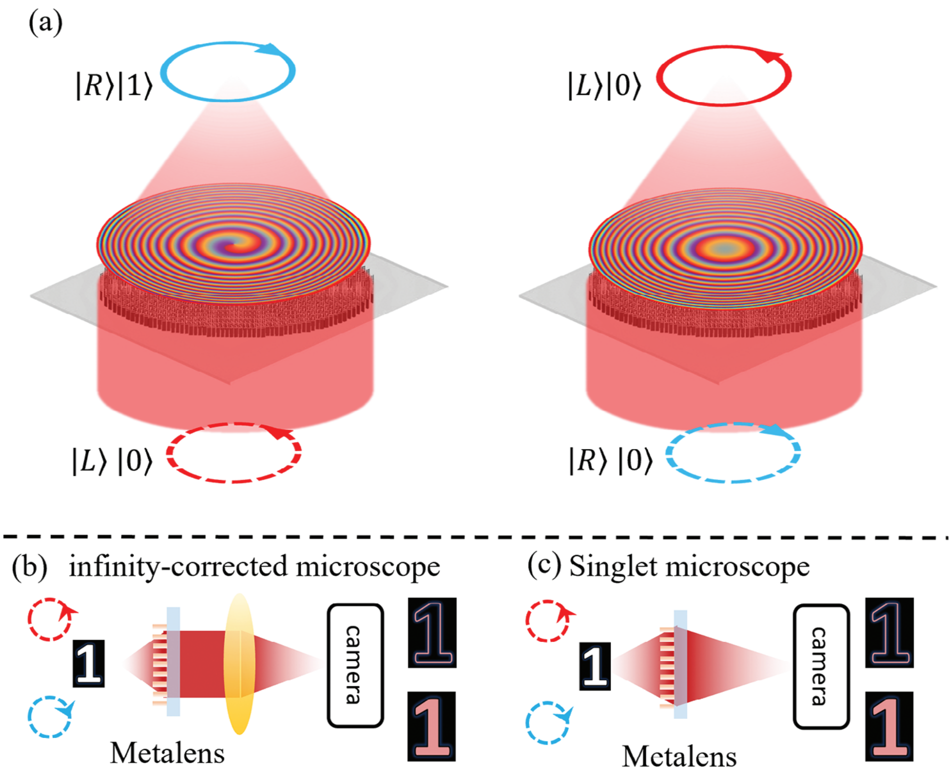

Figure 1. The concept of the polarization-controlled focusing and imaging mode. a) The principle of the polarization-controlled focusing mode. Metalens-based infinity-corrected microscope b) and singlet microscope c) for polarization-controlled phase contrast imaging and bright field imaging.

phase gradient microscopy is demonstrated by cascading two dedicated designed metasurfaces for direct edge-enhanced images of the phase-type object.[16] Nevertheless, it could not be used for amplitude-type objects, which limit its applications. In contrast, the spiral phase contrast microscope can obtain the edge-enhanced image of both phase and amplitude objects.[4,17] A single-metalens spiral phase contrast imaging configuration was achieved by compressing the imaging and edge-enhancement functionalities into one transmissive metalens in the visible spectrum.[17]

Recently, a dielectric metasurface has been proposed for synchronous spiral phase contrast and bright field imaging at the wavelength of 10.6 µm[18] with coherent light and visible spectrum with incoherent light.[4] While the large FOVs (~cm) are achieved in the two studies, their resolutions are 40[18] and 560 µm,[4] respectively, which are not suitable for microscopy observation. By incorporating a liquid crystal cell, an electrically tunable dual-mode metalens is reported for switchable spiral phase contrast and bright field imaging.[19] However, a low resolution $(\approx 3\lambda)$ with distorted edge-enhanced image[19] were demonstrated with limitations of the numerical aperture and the interference from a coherent light source. Partially coherent light sources such as light-emitting diodes (LED) are frequently used in semiconductor inspection and biological research (e.g., fluorescence). It is vital to demonstrate a metalens-based dual-mode imaging system with the illumination of partially coherent illumination for applications.

There is no report on the switchable dual-mode (i.e., bright field and phase contrast) microscope with high resolution $(<\lambda)$, large magnification, and large FOV. While the above metalenses work in the visible[4,19] and Mid-infrared spectrum,[18] the near-infrared (NIR) spectrum is attracting increasing attention in biological research, machine vision and semiconductor inspection because of several advantages. First, the NIR light wave can penetrate through the biological tissue deeper than visible light. Second, the visible auto-fluorescence of cells and tissues is considered the main source of background noise in biological imaging, imaging in NIR can achieve a higher signal-to-noise ratio.[20,21] Moreover, NIR microscopy provides defect information on the silicon chips compared to visible light for semiconductor inspection.

Here, we demonstrated polarization-controlled dual-mode imaging systems in the NIR imaging window based on partial coherent LED illumination. Our concept of a polarization-controlled single-layer dielectric metalens where the phase profile can be tuned from a hyperbolic phase to a sum of a hyperbolic phase and a spiral phase with a topologic charge of 1, as shown in **Figure 1**. At 1550 nm, the metalens can focus the left-handed circular polarized (LCP) light beam to a donut ring with a topologic charge of 1 for phase contrast imaging mode and focus the right-handed circular polarized (RCP) light beam to a Gaussian focal point for bright field imaging. Two metalens samples with a numerical aperture (NA) of 0.89 and 0.25 are fabricated and characterized in the

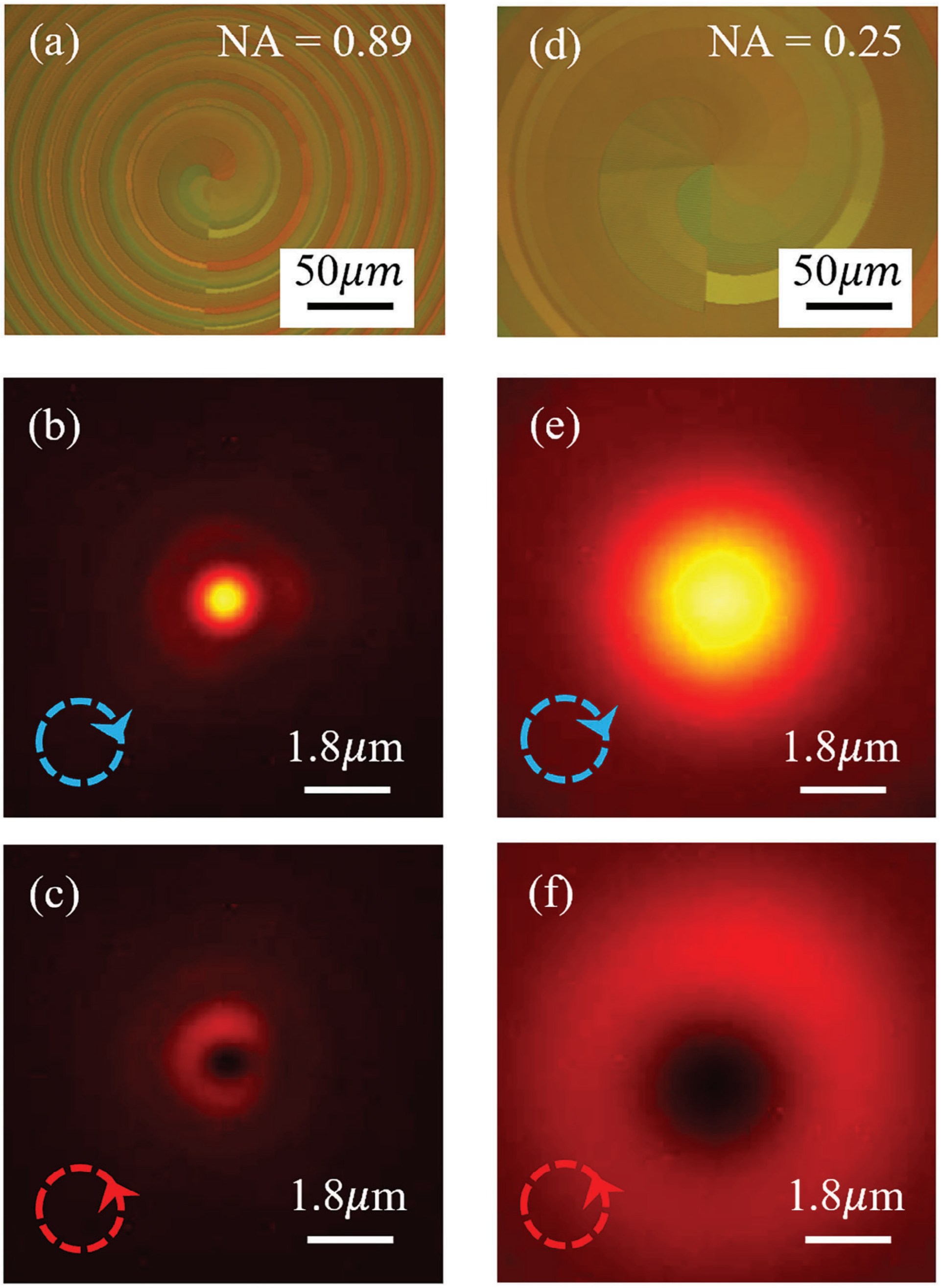

Figure 2. Characterization of metalenses. The (a–c) are the optical image, Gaussian focal point, and donut-shaped focal point of the metalens sample 1 (NA = 0.89), respectively; (d–f) are the optical image, Gaussian focal point, and donut-shaped focal point of the metalens sample 2 (NA = 0.25), respectively.

experiment, and polarization-controlled dual-mode microscopes are demonstrated.

2. Metalens Design and Characterization

We use the spin-multiplexing method imposing two distinct phase profiles on the LCP and RCP light beams in the same metalens, respectively. As shown in Figure 1a, to realize phase contrast imaging mode, the metalens impart a sum phase profile (Equation (1) of the hyperbolic phase and the spiral phase with a topological charge of 1 on the LCP light beam. A hyperbolic phase profile (Equation (2) is imparted onto the RCP light beam to realize bright field imaging mode. Therefore, the metalens in a microscope system can serve as an imaging lens and a polarization-controlled phase plate as shown in Figure 1b,c.

$$\Psi_L = \frac{2\pi}{\lambda}\left(f - \sqrt{f^2 + r^2}\right) + \Phi \tag{1}$$

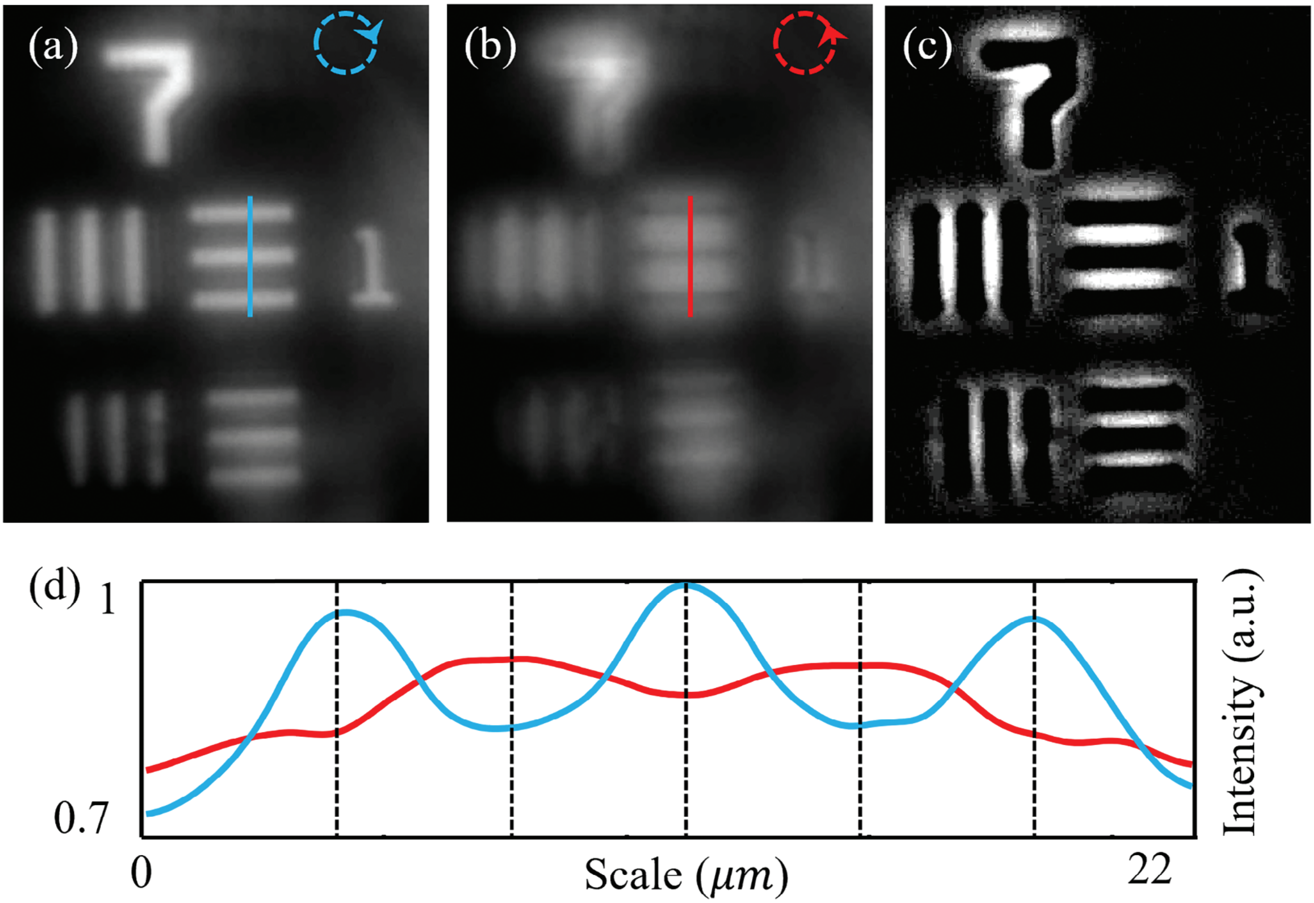

Figure 3. The imaging results of the 58X infinity-corrected microscope. (a) and (b) show the bright-field image and edge-enhanced image, c) is the differential image between the edge-enhanced image and the bright-field image, and d) demonstrates the intensity of the cut lines in (a,b).

$$\Psi_R = \frac{2\pi}{\lambda}\left(f - \sqrt{f^2 + r^2}\right) \tag{2}$$

Ψ_L (Equation (1) is the phase profile imparted on the incident LCP light beam and Ψ_R (Equation (2) is the phase profile imparted on the incident RCP light beam. f is the target focal length, and (r, Φ) is the polar coordinate of the nanofin overall metalens. As discussed in Figure S1 (Supporting Information), the propagation phase φ_x depends on the size (W_x and W_y) of the nanofin (Figure S1a, Supporting Information), and θ is the rotation angle of the nanofin, Figure S1b (Supporting Information). A library including eight nanofins in Figure S2d (Supporting Information) with height H of 800 nm and period P of 650 nm is designed to realize 2π phase coverage. The design details of the library can be seen in Sections S1 and S4 (Supporting Information).

Based on Equations (1) and (2), the target propagation phase profile φ_x can be confirmed, Equation S7 (Supporting Information). Combining the nanofins library in Figure S2d (Supporting Information), the size of nanofin at each lattice (r, Φ) is determined. From Equations (1) and (2), the rotation angle θ of the nanofin at each lattice (r, Φ) is determined as well, Equation S8 (Supporting Information). Repeating the above process at each lattice, the whole metalens is designed. A metalens was designed and fabricated with a diameter of 4 mm, NA of 0.89 and a focal length f of 1 mm shown in **Figure** 2a. The second metalens was designed and fabricated with a diameter of 4 mm, NA of 0.25 and a focal length f of 8 mm, as shown in Figure 2d.

The metalens samples were fabricated from the 800 nm a-Si film which is deposited on a SiO_2 substrate via plasma-enhanced chemical vapor deposition. The nanofins distribution were transferred to the a-Si film by using electron beam lithography, and the nanofins were etched by the reactive ion etcher. The fabrication details can be obtained from our recent publication.[22] Figure 2a,d are the optical images of the two metalen samples. In the following, sample 1 refers to the metalens with a target NA of 0.89, and sample 2 refers to the metalens with a target NA of 0.25.

A customized microscope with a magnification of 100X and NA of 0.9 was used to characterize the polarization-controlled focusing ability of the two samples (Figure S3, Supporting Information). The Gaussian focal point is first measured to evaluate the NA of two samples under the RCP beam illumination. The full width of half maximum (FWHM) of sample 1 is measured to be 1.1 μm, shown in Figure 2b, which demonstrates that sample 1 has an NA of 0.89. The FWHM of sample 2's Gaussian focal point is 3.8 μm corresponding to an NA of 0.25, Figure 2e. These results indicate that two diffraction-limited Gaussian

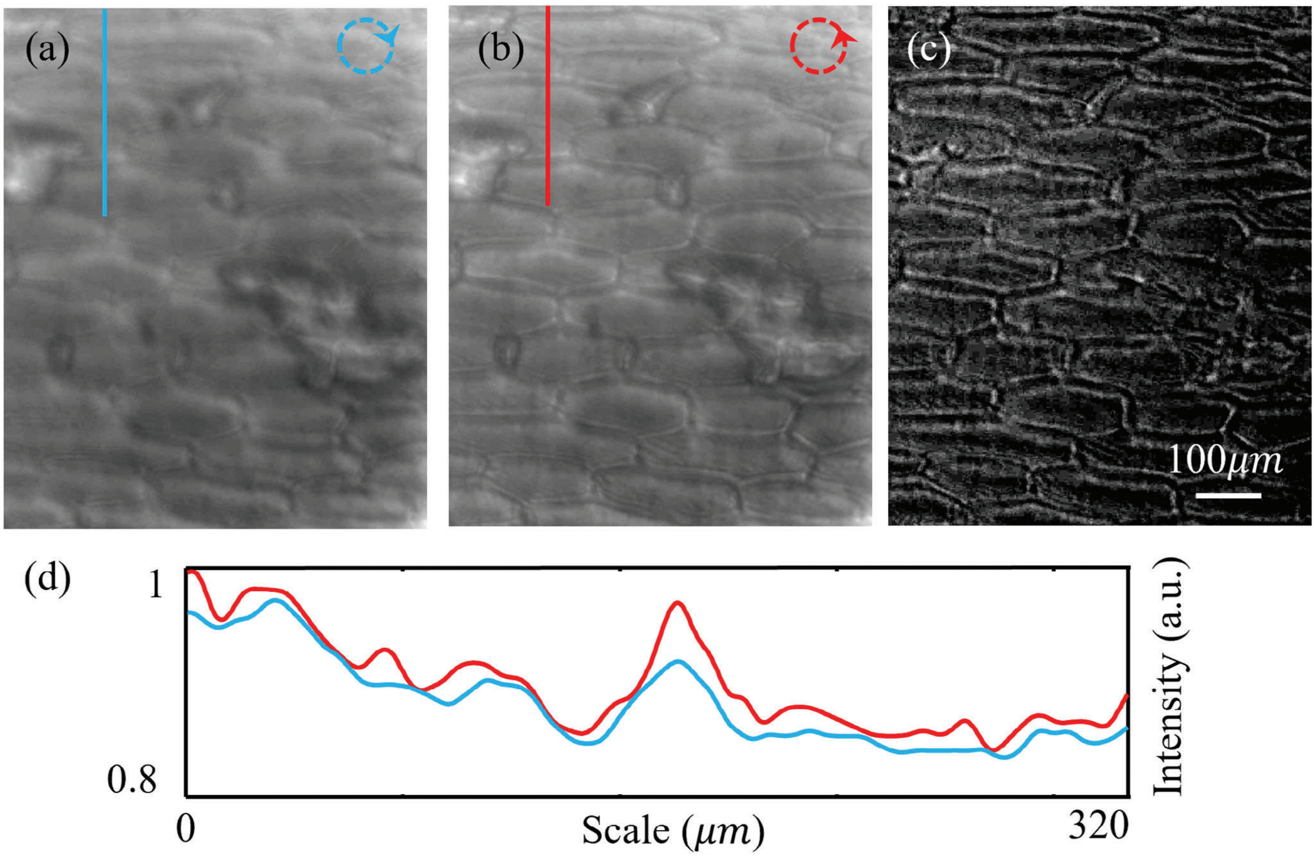

Figure 4. Biological imaging results for onion cells with the 7.8X microscope. a,b) show the bright-field image and edge-enhanced image, c) is the differential image, and d) demonstrate the intensity curve.

focal points are obtained by illuminating samples 1 and 2 via an RCP light beam. As shown in Figure 2c,f, the two Gaussian focal points were tuned to be two donut rings by changing the illumination light beam to LCP. Supporting video V1 shows the transition process of the focal field of metalens sample 1 by rotating a quarter waveplate (QWP), shown in Figure S3 (Supporting Information). The donut ring of sample 1 has a radius of 1.6 μm, and the donut ring of sample 2 has a radius of 5.7 μm, respectively. As the light energy is spread into a large donut ring with a Gaussian focal point, the intensity of the donut ring shown in Figure 2c,f is weaker than the intensity of the Gaussian focal points shown in Figure 2b,e, while the two focusing modes have similar efficiencies. Specifically, the efficiencies of Gaussian and donut focusing modes are 38.6% and 36.1%, respectively. The working efficiency can be effectively improved by introducing a toroidal response,[23] employing an inverse design approach,[24] and optimizing the fabrication process.

To realize a large-magnification (58X) and a high-resolution (0.7λ) dual-mode imaging system, an infinity-corrected microscope in Figure 1b was demonstrated by utilizing the metalens sample 1 as a high-NA objective lens (Section 3.1). A second infinity-corrected dual-mode microscope with large FOV (600 × 800 μm) and a diffraction-limited imaging resolution ($0.61\lambda/\text{NA}$) was demonstrated by utilizing the metalens sample 2 as the objective lens (Section 3.2). Finally, a singlet dual-mode microscope system in Figure 1c was demonstrated via the metalens sample 2 (Section 3.3).

3. Compact Dual-Mode Imaging Experiments

3.1. High-Resolution and Large Magnification Infinity-Corrected Microscope

An infinity-corrected microscope in Figure 1b was constructed by utilizing the metalens sample 1. The metalens serve as a high-NA (0.89) objective lens and polarization-controlled phase filter. A cemented achromatic doublets lens (Thorlabs, AC254-060-C) with a focal length of 60 mm is adopted as the tube lens. One polarizer and QWP are placed between the light source and the resolution target to manipulate the illumination light's polarization state. The image is captured by an InGaAs camera.

To avoid the imaging quality reduction induced by laser interference and directly realize the edge-enhancement effect in the imaging system, a partially coherent LED light source is used for illuminating the USAF 1951 resolution target. In addition, comparing the laser and ambient light, the coherence of the LED is similar to the coherence of the biological fluorescence. The utilization of LED makes our imaging system ready for biomedical imaging. However, the edge-enhancement effect would be weakened by lowering the coherence of the illumination light. We

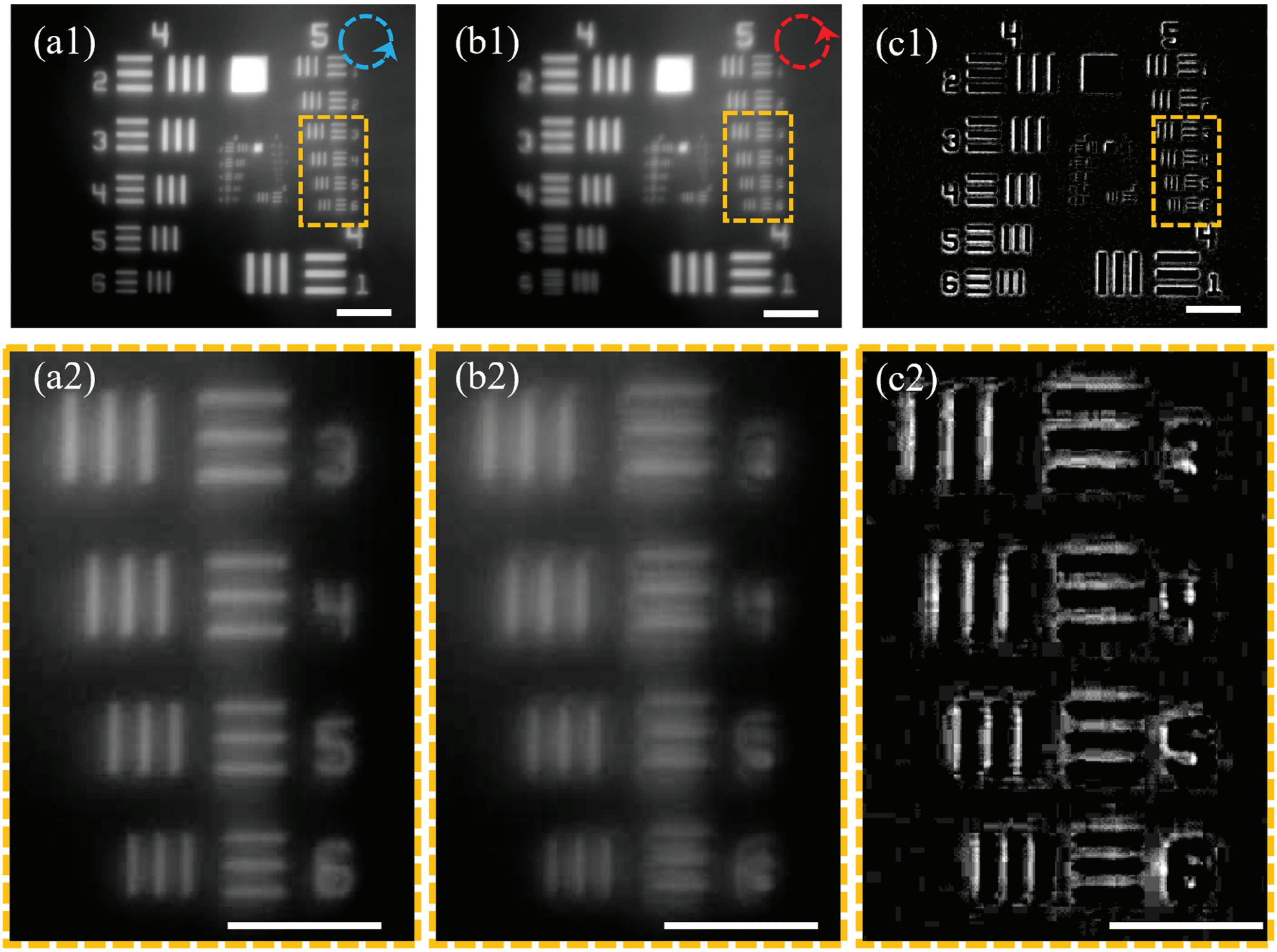

Figure 5. Imaging results of the singlet dual-mode microscope. (a) and (b) show the bright-field image and the edge-enhanced image, and c) is the differential image; The second row is the zoom-in figure of the first row. The scale bars in the first row are 200 µm, and the scale bars in the second row are 100 µm.

experimentally demonstrate that distinct edge images can be immediately achieved by subtracting the bright-field image from the edge-enhanced image.

Figure 3a,b shows the bright-field image and edge-enhanced image of element 1 in group 7, respectively. To quantitively demonstrate the transition of imaging mode, the intensity along the blue and red lines in Figure 3a,b are depicted in Figure 3d, which demonstrates the intensity peaks are tuned to the intensity valley with the imaging mode being tuned from bright-field to phase contrast imaging mode. A distinct edge of the object is obtained via the differential image (Figure 3c) via a one-step subtraction operation. According to the real dimension of element 1 in group 7, the magnification of our compact dual-mode microscope is calculated to be 58 times (i.e., 58X). The bright-field image and edge-enhanced image of the element 6 in group 7 indicate that the microscope could effectively resolve a feature size ≈1 µm in both bright field and phase contrast imaging mode, which means the microscope has a diffraction-limited sub-wavelength resolution ($0.61\lambda/\text{NA} = 0.7\lambda = 1.1\mu\text{m}$) at the wavelength of 1550 nm, shown in Figure S4a,b (Supporting Information). However, limited by the sensor size of the InGaAs camera, this microscope can only provide us with a small FOV (80 × 108 µm) in this configuration.

3.2. Diffraction-Limited Resolution and Large FOV Microscope for Biological Sample

We demonstrated the field of view of 600 × 800 µm, diffraction-limited image resolution, and biological dual-mode imaging by using the metalens sample 2 with a focal length of 8 mm and NA of 0.25 in our custom-built microscope. Figure S5 (Supporting Information) demonstrates the two different fields of view achieved by two samples. The imaging resolution and magnification of the second microscope are measured by capturing the dual-mode images of the group 7 in resolution target. Figure S4c,d (Supporting Information) respectively shows the bright-field image and edge-enhanced image of the group 7 in USAF 1951 resolution target. Therefore, the imaging magnification and resolution of this microscope are calculated to be 7.8X and 3.78 µm (i.e., diffraction limitation of the metalens sample 2, $0.61\lambda/\text{NA} = 2.44\lambda$).

A freshly peeled and unstained onion epidermal is prepared for verifying the dual-mode imaging ability of the microscope in biological samples. The cell wall (i.e., the edge of cells) becomes clear (**Figure** 4b) from blurred (Figure 4a) in whole FOV (600 × 800 µm) with the illumination light tuned to be LCP from RCP. The intensity along the blue and red lines in Figure 4a,b are depicted in Figure 4d to show the edge-enhancement effect quantitively. While the edge-enhancement effect of this biological experiment is not as clear as the USAF 1951 resolution target experiment, the onion cell's edges can be clearly observed in the differential image (Figure 4c). In theory, the FOV can be further enlarged by adopting a camera with a larger imaging sensor.

3.3. Singlet Dual-Mode Microscope

While edge detection plays an important role in a lot of industrial applications, the edge-detection is mostly achieved by post-processing of a bright-field image via software algorithms. The processing speed of current edge-detection algorithms highly depends on the computer hardware and software. If we directly get the edge-enhanced images of the target objects based on an all-optics system, the edge detection would be improved to be light speed, which would boost the industrial application. In addition, the imaging system should be simplified as much as possible to improve the system's robustness and reduce the cost. In the following, a singlet dual-mode microscope is demonstrated to realize all-optical edge detection at 1550 nm wavelength.

The metalens sample 2 is mounted 40 mm in front of the InGaAs camera sensor (i.e., the imaging distance is 40 mm) via a 3D-printed holder. The USAF 1951 resolution target is placed 10 mm in front of the metalens to get a clear image in the camera. **Figure** 5a1,b1 show the bright-field image and edge-enhanced image of the whole FOV, respectively. To show the resolution of the singlet microscope, the zoom-in figures of group 5 of USAF 1951 resolution target are shown in Figure 5a2,b2. According to the real dimension of element 5 in group 5 (Figure 5a2), the magnification of this singlet dual-mode microscope is calculated to be 4.2X. As the differential image Figure 5c shows, the edge can be quickly detected via one-step subtraction. Therefore, a fast edge-detection system with a simple hardware configuration is achieved in this research.

4. Conclusion

In summary, two compact dual-mode (i.e., phase-contrast and bright-field) microscope systems are demonstrated in the near-infrared spectrum based on silicon metalens. We first designed a bi-functional metalens that acts as a polarization-controlled phase plate and a high-NA objective lens. Two metalens samples with a diameter of 4 mm are fabricated, and two samples respectively have a NA of 0.89 and 0.25. After characterizing the diffraction-limited focusing performance of two samples, the dual-mode infinity-corrected microscope was demonstrated by using the metalenses as the objective lenses with a partially coherent LED light source. The microscope can realize a large magnification of 58X and a high resolution of 0.7λ for the metalens sample 1, and a large field of view of 600 × 800 µm is obtained by replacing sample 1 (NA 0.89) with sample 2 (NA 0.25). The edge-enhanced image of an unstained onion epidermal is observed by the microscope. Finally, a dual-mode singlet microscope is built based on sample 2 with NA of 0.25 for realizing fast edge detection. Our experiment results illustrate that the dual-mode microscope systems have enormous potential for applications in biomedical diagnosis, biological and chemical research, and the industrial fields of machine vision and safety monitoring.

Supporting Information

Supporting Information is available from the Wiley Online Library or from the author.

Acknowledgements

PhD studentship from the Chinese Scholarship Council is acknowledged. This work was supported by the UK's Engineering and Physical Sciences Research Council (project number EP/V000624/1, EP/X03495X/1, and EP/T02643X/1), the CHIST-ERA grant (project number CHIST-ERA-21-NOEMS-004) and supported by the Royal Society (project number RG\R2\232531).

Conflict of Interest

The authors declare no conflict of interest.

Data Availability Statement

The data that support the findings will be available in the University of Southampton's ePrints research repository: http://dx.doi.org/10.5258/SOTON/D3056.

Keywords

bright field image, edge detection, metalens, spiral phase contrast image

Received: February 22, 2024
Revised: April 21, 2024
Published online:

---

[1] Y. Z. Zhang, P. C. Lin, P. C. Huo, M. Liu, Y. Ren, S. Zeng, Q. Zhao, Y. Wang, Y.-Q. Lu, T. Xu, *Nano Lett.* **2023**, *23*, 2991.
[2] F. Zernike, *Science.* **1955**, *121*, 345.
[3] C. R. Bagnell, Chapter 10 Phase Contrast, US: UNC School of Medicine **2012**.
[4] S. Wang, L. Li, S. Wen, R. Liang, Y. Liu, F. Zhao, Y. Yang, *Nano Lett.* **2024**, *24*, 356.
[5] K. M. Taute, S. Gude, S. J. Tans, T. S. Shimizu, *Nat. Commun.* **2015**, *6*, 8776.
[6] S. Furhapter, A. Jesacher, S. Bernet, M. Ritsch-Marte, *Opt. Express.* **2005**, *13*, 689.
[7] J. K. Wang, W. H. Zhang, Q. Q. Qi, S. S. Zheng, L. X. Chen, *Sci. Rep.* **2015**, *5*, 15826.
[8] M. Y. Pan, Y. F. Fu, M. J. Zheng, H. Chen, Y. J. Zhang, *Light: Sci. Appl.* **2022**, *11*, 195.
[9] D. Jeon, K. Shin, S.-W. Moon, J. Rho, *Nano Convergence.* **2023**, *10*, 24.

[10] X. J. Zou, G. G. Zheng, Q. Yuan, W. Zang, R. Chen, T. Y. Li, S. Wang, Z. Wang, S. Zhu, *PhotoniX*. **2020**, *1*, 2.

[11] S. Banerji, M. Meem, A. Majumder, F. G. Vasquez, B. Sensale-Rodriguez, R. Menon, *Optica*. **2019**, *6*, 805.

[12] P. C. Huo, C. Zhang, W. Q. Zhu, M. Liu, S. Zhang, Si. Zhang, L. Chen, H. J. Lezec, A. Agrawal, Y. Q. Lu, T. Xu, *Nano Lett*. **2020**, *20*, 2791.

[13] T. F. Zhu, Y. H. Zhou, Y. J. Lou, H. Ye, M. Qiu, Z. C. Ruan, S. H. Fan, *Nat. Commun*. **2017**, *8*, 15391.

[14] T. F. Zhu, C. Guo, J. Y. Huang, H. Wang, M. Orenstein, Z. C. Ruan, S. H. Fan, *Nat. Commun*. **2021**, *12*, 680.

[15] Y. Zhou, H. Y. Zheng, I. I. Kravchenko, J. Valentine, *Nat. Photonics*. **2020**, *14*, 316.

[16] H. Kwon, E. Arbabi, S. M. Kamali, M. Faraji-Dana, A. Faraon, *Nat. Photonics*. **2020**, *14*, 109.

[17] Y. J. Kim, G. Y. Lee, J. W. Sung, J. H. Jang, B. G. Lee, *Adv. Funct. Mater.* **2022**, *32*, 2106050.

[18] Q. He, F. Zhang, M. B. Pu, X. L. Ma, X. Li, J. J. Jin, Y. H. Guo, X. G. Luo, *Nanophotonics*. **2021**, *10*, 741.

[19] T. Badloe, Y. Kim, J. Kim, H. Park, A. Barulin, Y. N. Diep, H. Chao, W.-S. Kim, Y.-K. Kim, I. Kim, J. S. Rho, *ACS Nano*. **2023**, *17*, 14678.

[20] X. X. Peng, X. F. Zhu, J. L. Zhang, *J. Inorg. Biochem*. **2020**, *209*, 111118.

[21] Z. Feng, T. Tang, T. X. Wu, X. Yu, Y. Zhang, M. Wang, J. Zheng, Y. Y. Ying, S. Chen, J. Zhou, X. X. Fan, D. Zhang, S. L. Li, M. Zhang, J. Qian, *Light: Sci. Appl*. **2021**, *10*, 197.

[22] C. Sun, H. L. Pi, K. S. Kiang, T. S. Georgescu, J.-Y. Ou, H. Ulbricht, J. Yan, *Nanophotonics*. **2024**, https://doi.org/10.1515/nanoph-2023-0873.

[23] A. Hassanfiroozi, Z. S. Yang, S. H. Huang, W.-Hui. Cheng, Y. Shi, P. C. Wu, *Adv. Opt. Mater.* **2023**, *11*, 2202717.

[24] C. H. Lin, Y. S. Chen, J. T. Lin, H.-T. Kuo, C.-F. Lin, P. Chen, P. C. Wu, *Nano Lett*. **2021**, *21*, 4981.